Dept. of Math. University of Oslo
Mechanics and Applied Mathematics No. 2
ISSN 0809–4403 December 2005

Variable depth and the validity of Boussinesq-type models

G. Pedersen

Abstract

The main issue of this report is comparison and verification of long wave models with emphasis on variable depth effects. A selection of dispersive long wave theories are reviewed. Included are the so-called standard Boussinesq equations and the much celebrated counterpart where the velocities are prescribed at an optimal vertical position, namely at 0.531 times the depth down from the equilibrium surface. The latter option, referred to as improved Boussinesq equations, displays substantially improved dispersion properties on constant depth. We also address formulations with the velocity potential as primary unknown and where approximations linked to a mild bottom slope have been invoked. One of the potential formulations are modified in a very simple way to yield dispersion properties equal to the "improved Boussinesq equations". First the different Boussinesq models are assessed for constant depth propagation. Then testing is extended to wave motion in an idealized bathymetry with two horizontal planes joined by a smooth slope. The length of the waves incident on the slope as well as the slope steepness are systematically varied.

It turns out that the new potential formulation, with improved dispersion properties, performs well even in presence of steep bottom gradients.

1 Introduction

Long wave theory have been an important tool for understanding the nature of water waves since the nineteenth century. Simplified descriptions of this type has allowed for a series of crucial analytic solutions, that offer insight to physical mechanisms, and have also been the basis for the vast bulk of models for tides, storm surges, tsunamis and oceanic circulations.

Over the last fifteen years we have observed a vital line of research that focus on the improvement of long wave theory with the eventual goal of closing the gap between shallow and deep water wave propagation models, in the sense that improved generalized long wave models might be valid for all waves long enough to be subjected to finite depth effects.

So far, most attention has been given to dispersion properties in constant depth and inclusion of a high degree of nonlinearity. Herein, the focus will be on variable depth effects and emphasis will be put on comparison with full,

albeit linear, potential theory. The potential solution is obtained by means of a boundary integral (BEM) technique, that is described in the appendix. Even though we employ a linear version only, the method is sketched for the full inviscid set.

2 Long wave equations

We employ a typical depth d and a wavelength L as vertical and horizontal length scales, respectively. The choice of L, in particular, is ambiguous and it may also correspond to other lengths than that of a wave. Identifying the time scale $t_c = L/\sqrt{gd}$, where g is the acceleration of gravity, and the dimensionless amplitude, ϵ, we define $\epsilon L/t_c$, $\epsilon d/t_c$ and ϵd, respectively, as scales for horizontal velocity, vertical velocity and surface elevation. Whereas the extraction of the amplitude factor, ϵ, is convenient for classification and description of long wave models, it will generally make results from computations less transparent. Hence, we will in graphs modify the scaling in a way that corresponds to putting $\epsilon = 1$ instead of invoking some amplitude measure.

Different long wave equations can be obtained through perturbation expansions in $\mu \equiv d/L$ and ϵ and may then be classified according to which orders of these parameters that are retained in the equations. Omission of all μ terms yields the nonlinear shallow water (NLSW) equations, while retaining second order in μ yields Boussinesq type equations that are available in a series of varieties[12, 13, 7]. Long wave theory prescribes a simple vertical structure of the field variables. In NLSW theory the horizontal velocity is vertically uniform and the pressure hydrostatic. Therefore, the vertical coordinate, z, vanishes from the equations. When $O(\mu^2)$ terms are retained there are vertical variations in the horizontal velocity. Still, the explicit appearance of z is removed from the continuity and momentum equations by integration. Hence, in this form they are often referred to as "depth integrated equations". The spatial dimension of the partial differential equations is then reduced by one. Furthermore, the nonlinear free surface appear only through nonlinear coefficients. These features make long wave formulations well suited for numerical solution. Regardless of the mathematical reduction of dimension, we will still refer to problems as two- or three dimensional according to the physical configuration.

The order of a long wave equation is reflected in the dispersion characteristics. According to full potential theory the dispersion relation of a linear, sinusoidal wave reads (depth: $h = 1$)

$$c^2 = \frac{1}{k\mu}\tanh(\mu k) = 1 - \frac{1}{3}(\mu k) + \frac{2}{15}(\mu k)^4 + ..., \qquad (1)$$

where c is the phase speed and k is the wave number. Shallow water theory only reproduces the first term on the right hand, while traditional Boussinesq equations yield the first two. However, as we will see below, different formulations valid to $O(\mu^2)$ give different dispersion properties. They may even reproduce the $O(\mu^4)$ term in (1) correctly or display en extended validity range.

2.1 Boussinesq theory

During the last fifteen years fully nonlinear Boussinesq type equations with improved dispersion properties have been put to work in computer models. Following [4] we write a set of fully nonlinear Boussinesq equations on the form

$$\eta_t = -\nabla \cdot \left[(h+\epsilon\eta)(\mathbf{v}+\mu^2\mathbf{M})\right] + O(\mu^4), \tag{2}$$

$$\mathbf{v}_t + \frac{\epsilon}{2}\nabla(\mathbf{v}^2) = -\nabla\eta - \mu^2\left[\frac{1}{2}z_\alpha^2\nabla\nabla\cdot\mathbf{v}_t + z_\alpha\nabla\nabla\cdot(h\mathbf{v}_t)\right] + \epsilon\mu^2\nabla(D_1+\epsilon D_2+\epsilon^2 D_3) + O(\mu^4) + \mathbf{N} + \mathbf{E}, \tag{3}$$

with

$$\begin{aligned}
\mathbf{M} &= \left[\frac{1}{2}z_\alpha^2 - \frac{1}{6}(h^2 - \epsilon h\eta + \epsilon^2\eta^2)\right]\nabla\nabla\cdot\mathbf{v} + \left[z_\alpha + \frac{1}{2}(h-\epsilon\eta)\right]\nabla\nabla\cdot(h\mathbf{v}),\\
D_1 &= \eta\nabla\cdot(h\mathbf{v}_t) - \frac{1}{2}z_\alpha^2\mathbf{v}\cdot\nabla\nabla\mathbf{v} - z_\alpha\mathbf{v}\cdot\nabla\nabla\cdot(h\mathbf{v}) - \frac{1}{2}(\nabla\cdot(h\mathbf{v}))^2,\\
D_2 &= \frac{1}{2}\eta^2\nabla\cdot\mathbf{v}_t + \eta\mathbf{v}\nabla\nabla\cdot(h\mathbf{v}) - \eta\nabla\cdot(h\mathbf{v})\nabla\cdot\mathbf{v},\\
D_3 &= \frac{1}{2}\eta^2\left[\mathbf{v}\cdot\nabla\nabla\cdot\mathbf{v} - (\nabla\cdot\mathbf{v})^2\right],
\end{aligned}$$

and where the index t denotes temporal differentiation, h is the equilibrium depth, η is the surface elevation, $\mathbf{v}$ is the horizontal velocity evaluated at $z = z_\alpha$ and ∇ is the horizontal component of the gradient operator. The heuristic terms $\mathbf{N}$ and $\mathbf{E}$ in the momentum equation (3) represent bottom drag and artificial diffusion, respectively. This particular form of the leading dispersion ($\epsilon^0\mu^2$) term was discussed and tested by [9], while additional nonlinearity was added by [3].

A similar formulation, with the velocity potential as primary unknown instead of the velocity, is found in [1]. Applying transformations and deletion of various higher order terms to the set (2) and (3) we may reproduce a number of other Boussinesq type equations from the literature[9, 3, 5]. As pointed out in the reference [3] weakly nonlinear versions, in the sense that some or all $O(\epsilon\mu^2)$ terms are omitted, may sometimes yield nonzero volume flux at the shoreline of a sloping beach. This should in particular be avoided for runup simulations.

When h is constant and $\epsilon \to 0$ Boussinesq equations on the form (2,3) yield c^2 as a rational function of μ^2k^2

$$c^2 = h\frac{1-\alpha\mu^2h^2k^2}{1+\beta\mu^2h^2k^2}, \tag{4}$$

where $\beta = -\frac{z_\alpha}{h} - \frac{z_\alpha^2}{2h^2}$ and $\alpha = \frac{1}{3} - \beta$. The latter identity assures that we always reproduce the $O((kh)^2)$ term in (1), regardless of the value of z_α. For $z_\alpha = (\sqrt{1/5} - 1)h$ the expression (4) reproduces the first three terms in the expansion (1), while $z_\alpha = -0.531h$ yields a particularly favourable dispersion relation over an extended range of wave numbers. (see Figs. 1 and 2). With $z_\alpha = (\sqrt{1/3} - 1)h$ the velocity $\mathbf{v}$ differs from the depth depth averaged velocity ($\overline{\mathbf{v}}$)

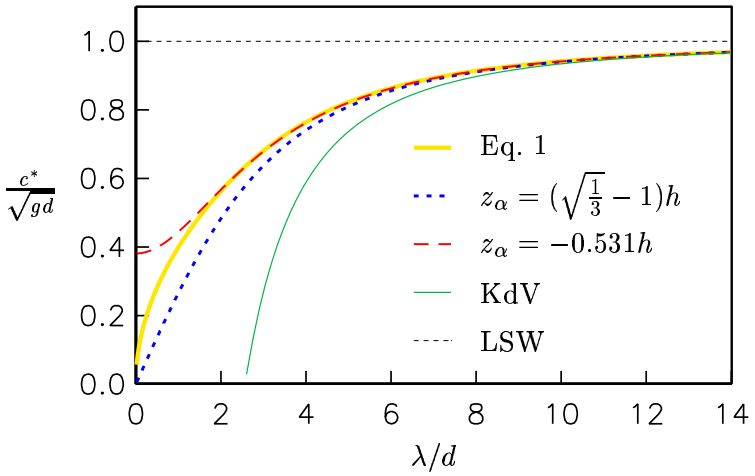

Figure 1: The phase speed as function of wavelength for long wave equations compared to that of the fully inviscid set. The curve for the Korteweg-deVries (KdV) equation is included for comparison.

by $O(\epsilon\mu^2)$, only. If we then delete all $O(\epsilon\mu^2)$ terms in (2) and (3) we retrieve the traditional Boussinesq equations for constant depth. These possess a dispersion relation that is clearly inferior to the optimal version of (2,3) (Fig. 1).

2.2 Standard and "mild-slope" Boussinesq equations

In general, the form of the volume flux in (2) implies[1] $\overline{\mathbf{v}} = \mathbf{v} + \mu^2\mathbf{M}$. Differentiating this relation with respect to time, inserting the resulting expression for $\mathbf{v}_t$ in (3), and invoking $\mathbf{v} = \overline{\mathbf{v}} + O(\mu^2)$ in nonlinear and dispersive terms we obtain the standard Boussinesq equations that inherit errors of order $\epsilon\mu^2, \mu^4$

$$\frac{\partial \eta}{\partial t} = -\nabla \cdot ((h + \epsilon\eta)\overline{\mathbf{v}}) \,, \tag{5}$$

$$\frac{\partial \overline{\mathbf{v}}}{\partial t} + \epsilon\overline{\mathbf{v}} \cdot \nabla\overline{\mathbf{v}} = -\frac{\partial \eta}{\partial x} + \frac{\mu^2}{2}h\nabla\nabla \cdot (h\frac{\partial \overline{\mathbf{v}}}{\partial t}) - \frac{\mu^2}{6}h^2\nabla^2\frac{\partial \overline{\mathbf{v}}}{\partial t} + O(\mu^4, \mu^2\epsilon) + \mathbf{N} + \mathbf{E}. \tag{6}$$

If we delete $\mathbf{N}$ and $\mathbf{E}$ we may invoke the depth averaged velocity potential and the standard Boussinesq equations take on the form [10, 6]

$$\frac{\partial \eta}{\partial t} = -\nabla \cdot \Big[(h + \epsilon\eta)\nabla\phi + \mu^2 G_2\Big] \,, \tag{7}$$

$$\frac{\partial \phi}{\partial t} + \frac{1}{2}\epsilon(\nabla\phi)^2 + \eta + \mu^2 G_1 = 0. \tag{8}$$

The terms G_1 and G_2 are dispersion terms that may be written according to

$$G_1 = -\frac{1}{2}h\nabla \cdot \nabla(h\frac{\partial \phi}{\partial t}) + \frac{1}{6}h^2\nabla^2\frac{\partial \phi}{\partial t}, \tag{9}$$

[1] To reproduce $\overline{\mathbf{v}}$ from $\mathbf{v}$ in non-constant depth we would have to employ a time dependent z_α.

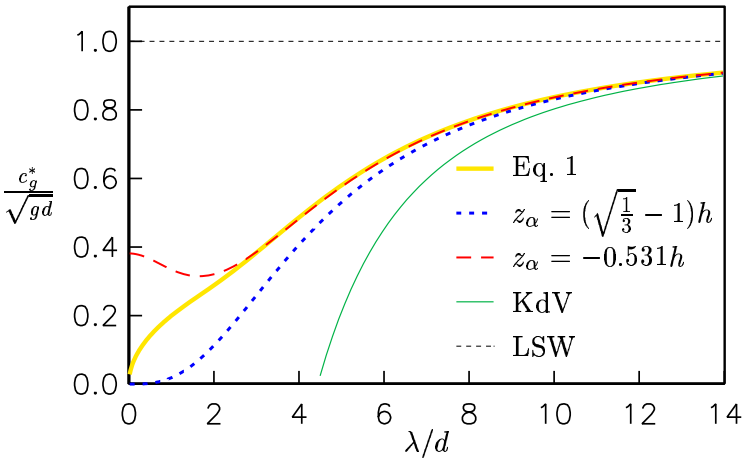

Figure 2: The group velocity as function of wavelength for long wave equations compared to that of the fully inviscid set. The curve for the Korteweg-deVries (KdV) equation is included for comparison.

$$G_2 = h\left(\frac{1}{6}\frac{\partial \eta}{\partial t} - \frac{1}{3}\nabla h \cdot \nabla \phi\right)\nabla h. \tag{10}$$

It must be emphasized that the sets (5,6) and (7,8) are far from equivalent, unless the depth is constant. The relation between the velocity and potential then reads

$$\overline{\mathbf{v}} = \nabla \phi, \tag{11}$$

and the formulations share the same curve in figure 1. However, in case of variable depth the relation between $\overline{\mathbf{v}}$ and ϕ is much more complex and the appearance of depth gradients in (7) and (8) is both inconvenient and prone to instabilities that are pursued in an ongoing parallel investigation. Assuming a mild bottom variation we may delete depth gradients in the dispersion terms and employ the simpler relations

$$G_1 = -\frac{1}{3}h^2\nabla^2\frac{\partial \phi}{\partial t}, \quad G_2 = 0. \tag{12}$$

In view of the approximations implicit in (12) it is now consistent to employ the relation (11) also for non-constant depth.

Subsequently we will refer to the set (5) and (6) as the standard Boussinesq equations, while (7) and (8) with (12) will be denoted as "mild" or "mild-slope" Boussinesq equations. The latter formulation is, maybe, the simplest Boussinesq equation that can be employed for propagation of nonlinear and weakly dispersive waves.

2.3 Potential formulations with improved dispersion properties

Staying with a mild-slope approximation the formulation of Chen and Liu (1995)[1] corresponds to

$$G_1 = \left(\frac{1}{2}z_\alpha^2 + z_\alpha h\right)\nabla^2\frac{\partial\phi}{\partial t}, \tag{13}$$

$$G_2 = -h\left(\frac{1}{6}h^2 - \frac{1}{2}(z_\alpha + h)^2\right)\nabla^3\phi, \tag{14}$$

where ϕ now is the value of the potential at vertical location z_α. With these dispersion terms we reproduce (4). The cost is the appearance of a fourth derivative of the potential in the continuity equation.

An alternative is to stick with the depth averaged potential and rewrite the dispersion term G_1 by means of $\partial\phi/\partial t + \eta = O(\mu^2, \epsilon)$:

$$G_1 = \gamma h^2\nabla^2\eta - (\frac{1}{3} - \gamma)h^2\nabla^2\frac{\partial\phi}{\partial t}, \quad G_2 = 0, \tag{15}$$

where the factor γ may be used to optimize the dispersion properties, in analogy to z_α. We again obtain a dispersion relation of the form (4) with $\alpha = \gamma$. Hence, we have dispersion properties identical to those of (2,3) when

$$\gamma = \frac{1}{3} + \frac{z_\alpha}{h} + \frac{1}{2}\frac{z_\alpha^2}{h^2} \tag{16}$$

The optimal value $z_\alpha = -0.531h$ then corresponds to $\gamma = -0.057$.

One might be tempted to combine the potential at z_α with a modification like (15) of the dispersion term of the momentum equation. The dispersion relation would then take on the form

$$c^2 = h\frac{1 - \alpha\mu^2h^2k^2 + \kappa\mu^4h^4k^4}{1 + \beta\mu^2h^2k^2}, \tag{17}$$

where we still have $\alpha = \frac{1}{3} - \beta$. Unfortunately, (17) is an unsound expression. If $\kappa < 0$ the nominator becomes negative for large k with resulting instability. On the other hand, if $\kappa > 0$ $c \to \infty$ as $k \to \infty$ which is another undesirable property.

2.4 Shallow water equations

Deletion of all $O(\mu^2)$ terms simplifies (2,3) to the NLSW equations. The pressure gradient in the momentum equation then becomes $\nabla\eta$, corresponding to hydrostatic pressure. As a consequence the horizontal velocity becomes independent of z. The NLSW equations lack the important effect of wave dispersion and may lead to erroneous results for long term propagation, even if the waves are long compared to the depth[12]. However, they are still a quite reasonable option for surf zone dynamics and are, by far, the most commonly used framework for runup calculations, as well as tsunami and storm surge models.

If the NLSW equations are linearized to yield the LSW equations, we may eliminate the velocity to obtain the standard wave equation

$$\eta_{tt} - \nabla\cdot(h\nabla\eta) = 0. \tag{18}$$

2.5 The numerical solution of long wave models

All long wave equations are solved by a centered finite difference methods that are described in [6] and [11]. These methods are of second order accuracy, but correction terms are designed to counteract leading effects of numerical dispersion. When these terms are active, the performance should roughly correspond to higher order Boussinesq discretizations from the literature. Anyhow, in the 2-D problems solved herein computational efficiency is not an important issue.

3 The test case

We invoke a simple test bathymetry, consisting of two uniform depth regions, with non-dimensional depths 1 and h_r, respectively, smoothly joined by

$$h(x) = \begin{cases} 1 & \text{if } x < x_a, \\ 1 + \frac{(h_r-1)}{2}\left(1 - \cos\left(\frac{\pi(x-x_a)}{\ell}\right)\right) & \text{if } x_a < x < x_a + \ell, \\ h_r & \text{if } x > x_a + \ell. \end{cases} \tag{19}$$

Varying the parameters h_r and ℓ we may produce cases that are more or less challenging concerning the effects of bottom gradients and wave dispersion. Generally, the length x_r should be half the wavelength, at least.

The wave propagation is started from rest with an initial elevation in the shape of half a bump adjacent to the left boundary.

$$\eta(x,0) = \begin{cases} 2A\cos^2\left(\frac{\pi x}{\lambda}\right) & \text{if } 0 < x < \frac{1}{2}\lambda, \\ 0 & \text{if } x > x_r. \end{cases} \tag{20}$$

In linear shallow water theory this will give rise to a wave of length λ and amplitude A. Naturally, the effect of dispersion will increase with decreasing λ.

4 Error estimates

For wave propagation it is not trivial to define the optimal error norm between two solutions. In a mathematical context the standard choice is some quadratic integrated norm, such as L_2. However, for long term wave propagation this may be quite inappropriate, due to accumulated errors in the phase. In fact, according to the L_2 norm two solutions of similar amplitude and shape, but large phase errors, may be more different than either of the solutions and the trivial zero field. Still, for even slightly complex wave patterns alternatives like maximum amplitude etc. are even more unsatisfactorily. In the present investigation we study the evolution of an initial pulse over a rather short propagation distance, including a sloping region. The solution will generally consist of a leading pulse, that in constant depth would approach an asymptote given by the Airy function, and a small residual wave train that may be qualitatively different for the various models. Deviations in both should contribute to a defined error. In this case the L_2 norm is probably a sensible choice, at last in want of a better alternative.

When a discrete quantity, γ_j, is defined on a grid, x_j ($j = 1..n$), the L_2 norm is defined as

$$\mathrm{L}_2(\gamma) = \sqrt{\sum_{j=1}^{n} \Delta x_j (\gamma_j)^2}, \tag{21}$$

where the increments, Δx_j, must be adequately defined, for instance as $\Delta x_j = \frac{1}{2}(x_{j+1} - x_{j-1})$. At the boundaries special care must be exercised concerning proper calculation of the contribution to the norm. Normally, we will report normalized norms of the deviations between the different solutions with emphasis on differences in the propagation properties. In these cases the boundary contributions may as well be left out.

We need to compute the deviation between discrete quantities, γ and κ, that are defined on different grids. Interpolation is then employed to calculate values $\hat{\kappa}$, of the latter, on the grid associated with γ. In case two solutions of the boundary integral method are compared we use spline interpolation that is consistent with the method itself. Otherwise, piecewise linear interpolation is invoked. The normalized deviation is then defined as

$$D(\gamma, \kappa) = \frac{\mathrm{L}_2(\gamma - \hat{\kappa})}{\mathrm{L}_2(\gamma)}. \tag{22}$$

When this procedure is employed to solutions from the same model, but with different grids, it is expressed as $D(\Delta x_1, \Delta x_2)$. It must be noted that while D is sensible as a measure of differences between converged solutions, it may become dominated by interpolation errors when applied as a measure of difference between numerical solutions obtained with different resolutions or grids. The use of $D(\Delta x_1, \Delta x_2)$ is then mainly to assure that errors of both numerics and interpolation are small enough to allow for a proper comparison of the outcome of solving different sets of *equations*.

5 Simulations, comparisons

5.1 Constant depth

For a start it is useful to study the case $h = 1$, meaning propagation in constant depth. In the linear case all evolution of shape is then due to dispersion and the wave-patterns will, in principle, consist of two parts. First, we have the front of the wave train, which in this case is an elevation. Secondly, there is a train of trailing waves with a significance that depends strongly on λ and the propagation distance. For both parts of the patterns simple asymptotic solutions are available for $t \to \infty$ (consult a good textbook like [8]). The asymptote of the front reads ($h = 1$)

$$\eta \sim \frac{\frac{1}{2}V}{(\frac{1}{2}t)^{\frac{1}{3}}} \mathrm{Ai}\left(\frac{x - t}{(\frac{1}{2}t)^{\frac{1}{3}}}\right), \tag{23}$$

where $V = \int_{-\infty}^{\infty} \eta(x, 0) dx$ and Ai is the Airy function. This solution is common for all equations that reproduce the leading dispersion correctly. Hence, different varieties of Boussinesq equations and potential theory will differ only in the transient evolution leading up to the asymptote.

However, the behaviour of the wave train will depend strongly on the group velocity, that is shown in figure 2. From the figure we see that the standard Boussinesq equations underestimate the group velocity dramatically for the shorter waves, while the improved version is good until $\lambda = 2$, say. For slightly smaller λ the group velocity of the improved Boussinesq equations reaches a minimum $c_g^{\min} = 0.315c_0$ at $\lambda^{\min} = 1.65d$ and then grows slightly to a value of $c_g^0 = 0.381c_0$ as $\lambda \to 0$. We observe that the limiting shallow water wave speed, c_0, equals unity when $h = 1$. In the large time asymptote the evolution is given by the well known stationary phase approximation to the Fourier integral. The dominant contribution to the solution at (x, t) then comes from the part of the spectrum in the vicinity of the wavenumber fulfilling

$$c_g(k) = \frac{x}{t}, \tag{24}$$

and reads

$$\eta(x,t) \sim \mathrm{Re}\, \frac{\tilde{\eta}_0(k)}{\sqrt{2\pi|\chi''(k)|}} \mathrm{e}^{\mathrm{i}(\chi(k) \pm \frac{\pi}{4})}. \tag{25}$$

The function $\tilde{\eta}_0$ is the Fourier transform of the initial elevation, the phase-function is defined as

$$\chi(k) = kx - \omega(k)t,$$

and the sign in the exponent equals the sign of χ'' (differentiation with respect to k). The formula (25) is indeed simple, but the solution of (24) in terms of k cannot be obtained in closed form for potential theory nor improved Boussinesq equations. The solution may of course be obtained numerically, but instead we prefer to regard (24) as a set of linear characteristics in the (x, t) plane, fanning out from the origin, along which k is preserved. The formula (25) then has the interpretation that the energy too moves with group velocity. From the specter, it is then straightforward to compute an unevenly distributed x, η dataset for each t. For the improved Boussinesq equations this procedure should, in principle, be modified for $x < c_g^0 t$. For smaller x, but still larger than $x < c_g^{\min} t$, we must add the stationary contributions from either side of $\lambda^{\min}$. At $x = c_g^0 t$ we have a double stationary point that must be handled in somewhat similar fashion as the wave front. It is not worthwhile to work out these marginal features of the improved Boussinesq solution.

As seen in figure 3 both the standard and improved Boussinesq equations are very good for $\lambda_0 = 24$. Even the LSW equations shows only a small L_2 deviation for this case. For $\lambda_0 = 8$ the wavy tail becomes apparent and the LSW equations fall short, while the improved Boussinesq equations are more accurate than the standard set. Anyhow, both are rather good (figure 5). The standard Boussinesq set over-predicts the extension of the tail severely for the short initial disturbance, $\lambda_0 = 3$ (figures 5 and 6). This is due to the underestimation of the group velocity that causes the energy of the short waves to move too slowly, in accordance with the stationary phase approximation. On the other hand, the improved Boussinesq formulation is still very good, but loses the rear part of the wave train due to the minimum for c_g.

It is instructive to observe how well the stationary phase approximation reproduces the wave trains quantitatively. Figure 7 shows that it does this

excellently for $\lambda_0 = 3$ and moderately large times. The stationary phase approximation is very close to the numerical solution from the leading peak and almost to the end of the wave-train, with exception of the irregular tail of the improved Boussinesq solution (see above).

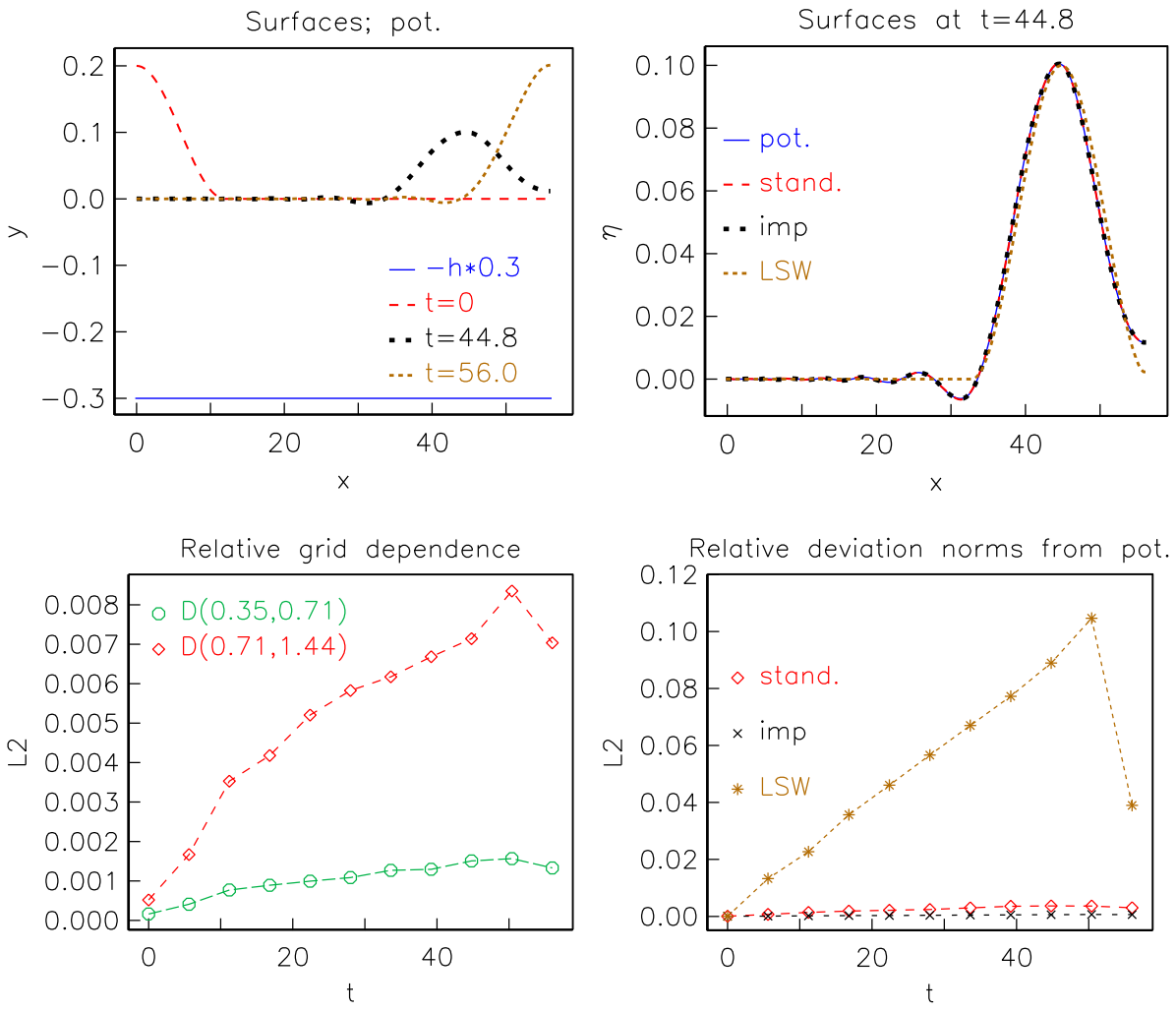

Figure 3: Comparison of linear Boussinesq and full potential models for $\boldsymbol{A = 0.2}$, $\boldsymbol{\lambda = 24.0}$, $\boldsymbol{\ell = 20}$, $\boldsymbol{h_r = 1}$, $\boldsymbol{x_r = 18.0}$, $\boldsymbol{x_{\max} = 56.0}$, $\boldsymbol{\Delta x = 0.35}$ (stand.). Upper left panel: surfaces at given times and the bottom. Upper right panel: comparison of different solvers at $t = 44.8$. Lower left panel: convergence of potential model; evolution of relative errors. Lower right panel: difference between other models and the potential theory.

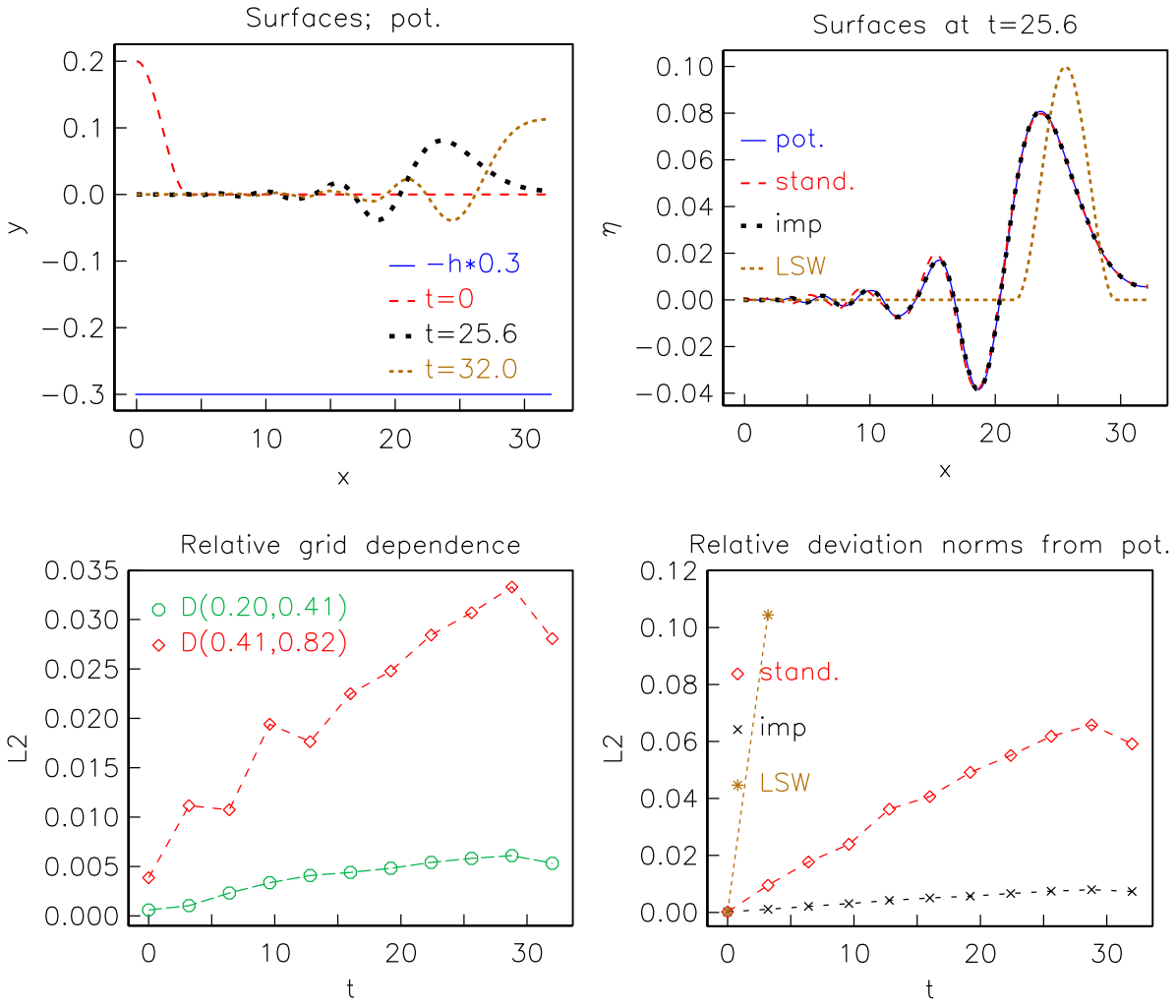

Figure 4: Comparison of linear Boussinesq and full potential models for $\boldsymbol{A = 0.2}$, $\boldsymbol{\lambda = 8.0}$, $\boldsymbol{\ell = 20}$, $\boldsymbol{h_r = 1}$, $\boldsymbol{x_r = 6.0}$, $\boldsymbol{x_{\max} = 32.0}$, $\boldsymbol{\Delta x = 0.20}$ (stand.). Upper left panel: surfaces at given times and the bottom. Upper right panel: comparison of different solvers at $t = 25.6$. Lower left panel: convergence of potential model; evolution of relative errors. Lower right panel: difference between other models and the potential theory.

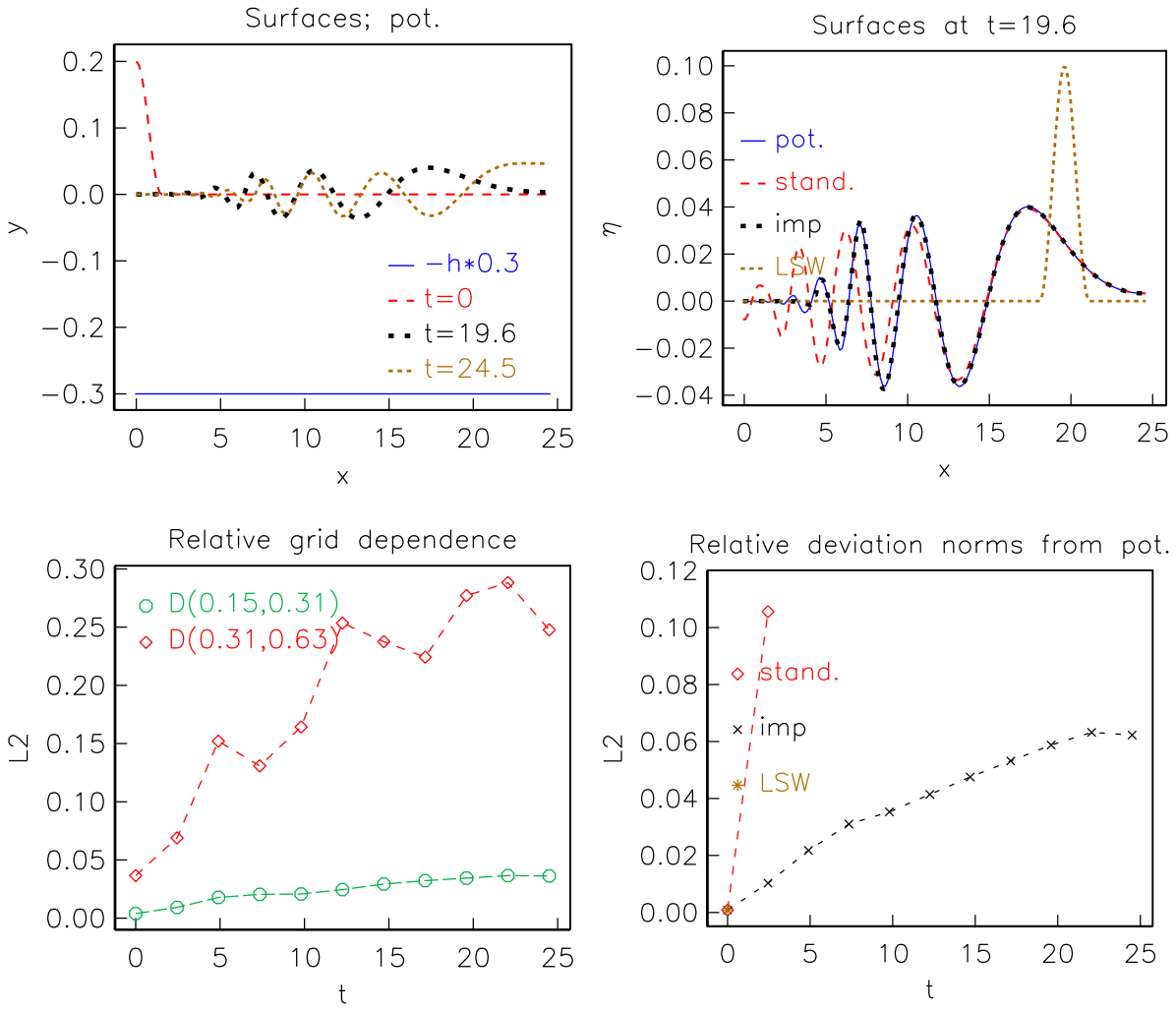

Figure 5: Comparison of linear Boussinesq and full potential models for $\boldsymbol{A} = \mathbf{0.2}$, $\boldsymbol{\lambda} = \mathbf{3.0}$, $\boldsymbol{\ell} = \mathbf{20}$, $\boldsymbol{h_r} = \mathbf{1}$, $\boldsymbol{x_r} = \mathbf{2.2}$, $\boldsymbol{x_{\max}} = \mathbf{24.5}$, $\boldsymbol{\Delta x} = \mathbf{0.15}$ (stand.). Upper left panel: surfaces at given times and the bottom. Upper right panel: comparison of different solvers at $t = 19.6$. Lower left panel: convergence of potential model; evolution of relative errors. Lower right panel: difference between other models and the potential theory.

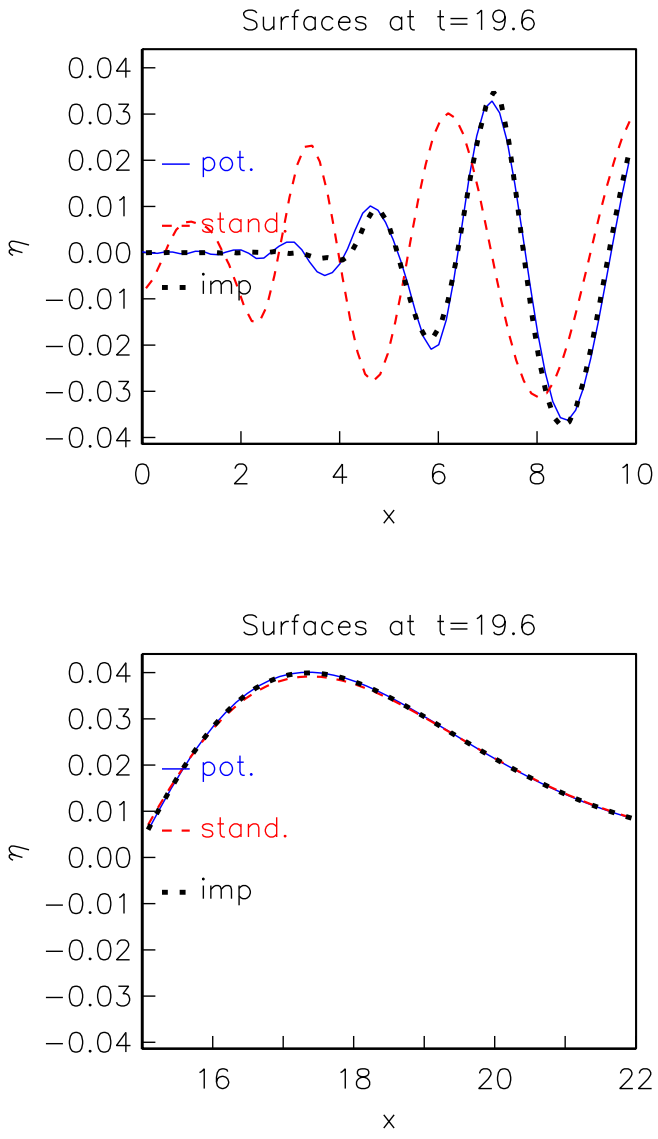

Figure 6: Closeup on tail and front for $a = 0.2$, $\lambda = 3.0$.

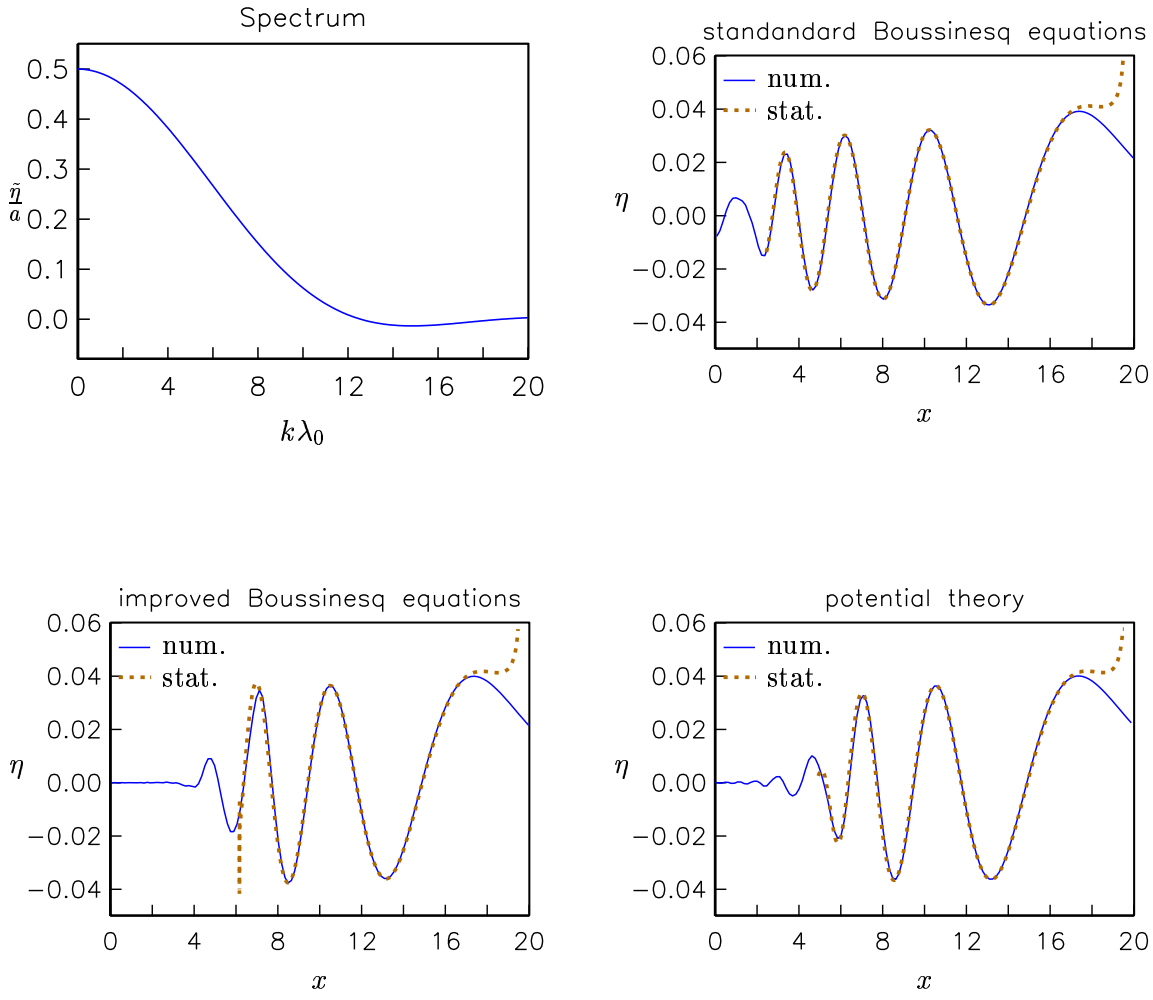

Figure 7: Validity of stationary phase. $a = 0.2$, $\lambda_0 = 1.5$, $\Delta x \sim 0.15$, $t = 19.6$.

	$\lambda = 3.0$	$\lambda = 6.0$	$\lambda = 8.0$	$\lambda = 24.0$
$\ell = 2$	0.36 0.27	0.19 0.12	0.14 0.07	0.03 0.01
$\ell = 3.5$	0.37 0.32	0.14 0.10	0.10 0.06	0.02 0.01
$\ell = 5$	0.40 0.36	0.13 0.10	0.09 0.06	0.02 0.01
$\ell = 10$	0.51 0.49	0.13 0.12	0.07 0.06	0.01 0.01
$\ell = 20$	0.66 0.67	0.17 0.17	0.09 0.08	0.01 0.01

Table 1: Maximum relative deviation, in L_2 norm, between linear Boussinesq models (mild., stand.) and the potential model for $h_r = 2$ and $\Delta x = 0.40$ (mild.).

5.2 Propagation over shelf

For variable bottom the deviations between the four Boussinesq type equations and potential theory are computed for a selection of wavelengths and slope widths, whereas the depth after the slope is $h_r = 2$ in all cases. To summarize the performance the maximum value of the relative deviation, D, is extracted for each Boussinesq model and tabulated. Table 1 contains results for the standard Boussinesq equations (5) and (6), marked by stand., and the mild slope equations (7), (8) and (12), marked by mild. Correspondingly, errors for the improved system (2) and (3) with $z_\alpha = -0.531h$, marked imp., are found in table 2, together with errors for the improved mild-slope formulation, (7), (8) and (15) with $\gamma = -0.057$, that are marked gam.

For the longest wavelength, $\lambda = 24$, the mild-slope Boussinesq models with standard dispersion properties (table 1) display a very weak increase in error as ℓ decreases. The standard version yields no significant increase in error even for $\ell = 2$. For the shorter wavelength there is no systematic increase with sharpening the depth gradient, because the total propagation distance is shortened accordingly which implies reduced effect of dispersion. Clearly, the deviations for the shorter wavelengths are more influenced by dispersion than by bottom gradients.

Concerning the equations with improved dispersion properties (table 2) the mild-slope version yields generally larger deviations, but the difference is not large. For $\lambda = 3$ the deviations are substantially smaller than for the standard Boussinesq equations.

A selection of surfaces and time stories of errors are given in the figures 8 through 13. We observe that there are some differences between the Boussinesq solvers concerning the evolution and distribution of deviations from fully dispersive solutions, however, none of which seems important.

6 Concluding remarks

We have tested four different Boussinesq models by comparison to fully dispersive solutions

1. Standard model with velocities as primary unknowns

2. Improved dispersion model with velocities as primary unknowns

	$\lambda = 3.0$	$\lambda = 6.0$	$\lambda = 8.0$	$\lambda = 24.0$
$\ell = 2$	0.14 0.11	0.13 0.09	0.11 0.06	0.02 0.01
$\ell = 3.5$	0.10 0.08	0.09 0.07	0.08 0.05	0.02 0.01
$\ell = 5$	0.09 0.07	0.07 0.06	0.06 0.05	0.02 0.01
$\ell = 10$	0.08 0.09	0.06 0.06	0.04 0.05	0.01 0.01
$\ell = 20$	0.09 0.14	0.05 0.08	0.04 0.06	0.01 0.01

Table 2: Maximum relative deviation, in L_2 norm, between linear Boussinesq models (gam., imp.) and the potential model for $h_r = 2$ and $\Delta x = 0.40$ (gam.).

3. Standard model with potential as unknown and mild bottom variation

4. Improved dispersion model with potential as unknown and mild bottom variation

We note that last option is suggested herein and do not correspond to the formulation of [1].

As expected the improved dispersion models are substantially better for short waves. For propagation over a slope the mild-slope versions perform nearly as well as their general-slope counterparts. Hence, as long as rotational effects can be ignored the simple equations, enumbered 4 in the list, appear to provide an attractive alternative for ocean modeling.

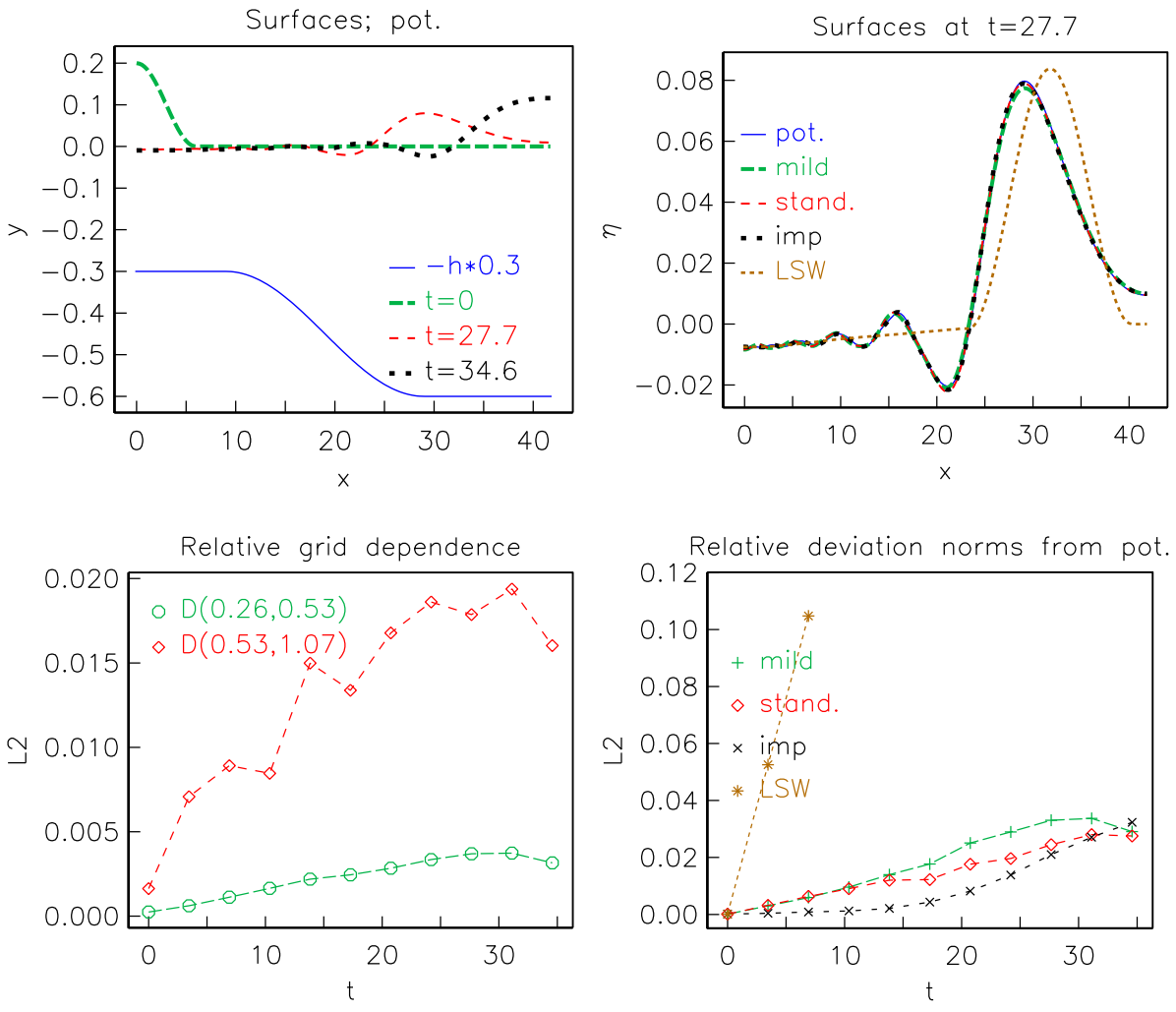

Figure 8: Comparison of linear Boussinesq and full potential models for $\boldsymbol{A = 0.2}$, $\boldsymbol{\lambda = 12.0}$, $\boldsymbol{\ell = 20}$, $\boldsymbol{h_r = 2}$, $\boldsymbol{x_r = 9.0}$, $\boldsymbol{x_{\max} = 41.7}$, $\boldsymbol{\Delta x = 0.26}$ (mild). Upper left panel: surfaces at given times and the bottom. Upper right panel: comparison of different solvers at $t = 27.7$. Lower left panel: convergence of potential model; evolution of relative errors. Lower right panel: difference between other models and the potential theory.

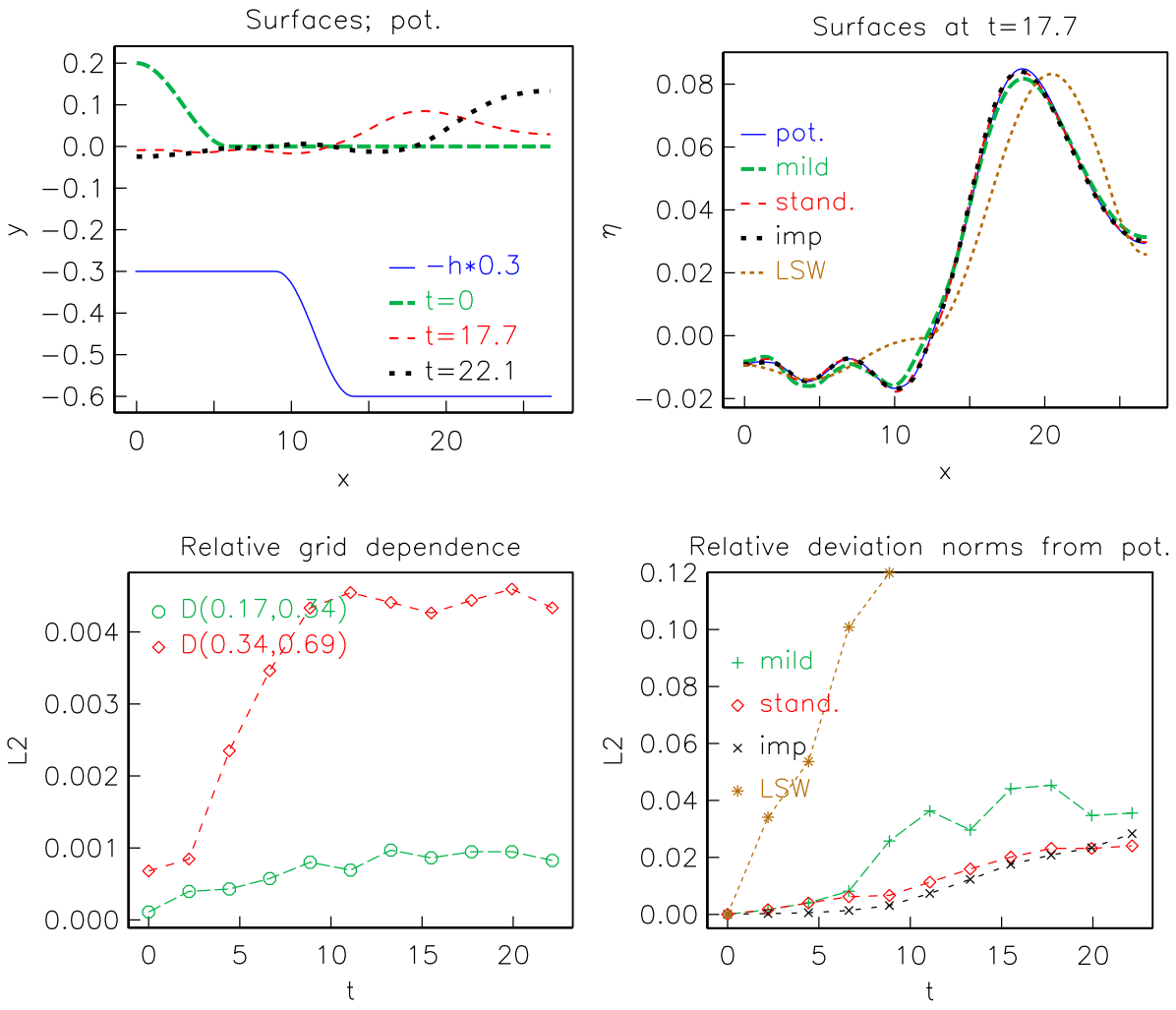

Figure 9: Comparison of linear Boussinesq and full potential models for $\boldsymbol{A} = \mathbf{0.2}$, $\boldsymbol{\lambda} = \mathbf{12.0}$, $\boldsymbol{\ell} = \mathbf{5}$, $\boldsymbol{h_r} = \mathbf{2}$, $\boldsymbol{x_r} = \mathbf{9.0}$, $\boldsymbol{x_{\max}} = \mathbf{26.7}$, $\boldsymbol{\Delta x} = \mathbf{0.17}$ (mild). Upper left panel: surfaces at given times and the bottom. Upper right panel: comparison of different solvers at $t = 17.7$. Lower left panel: convergence of potential model; evolution of relative errors. Lower right panel: difference between other models and the potential theory.

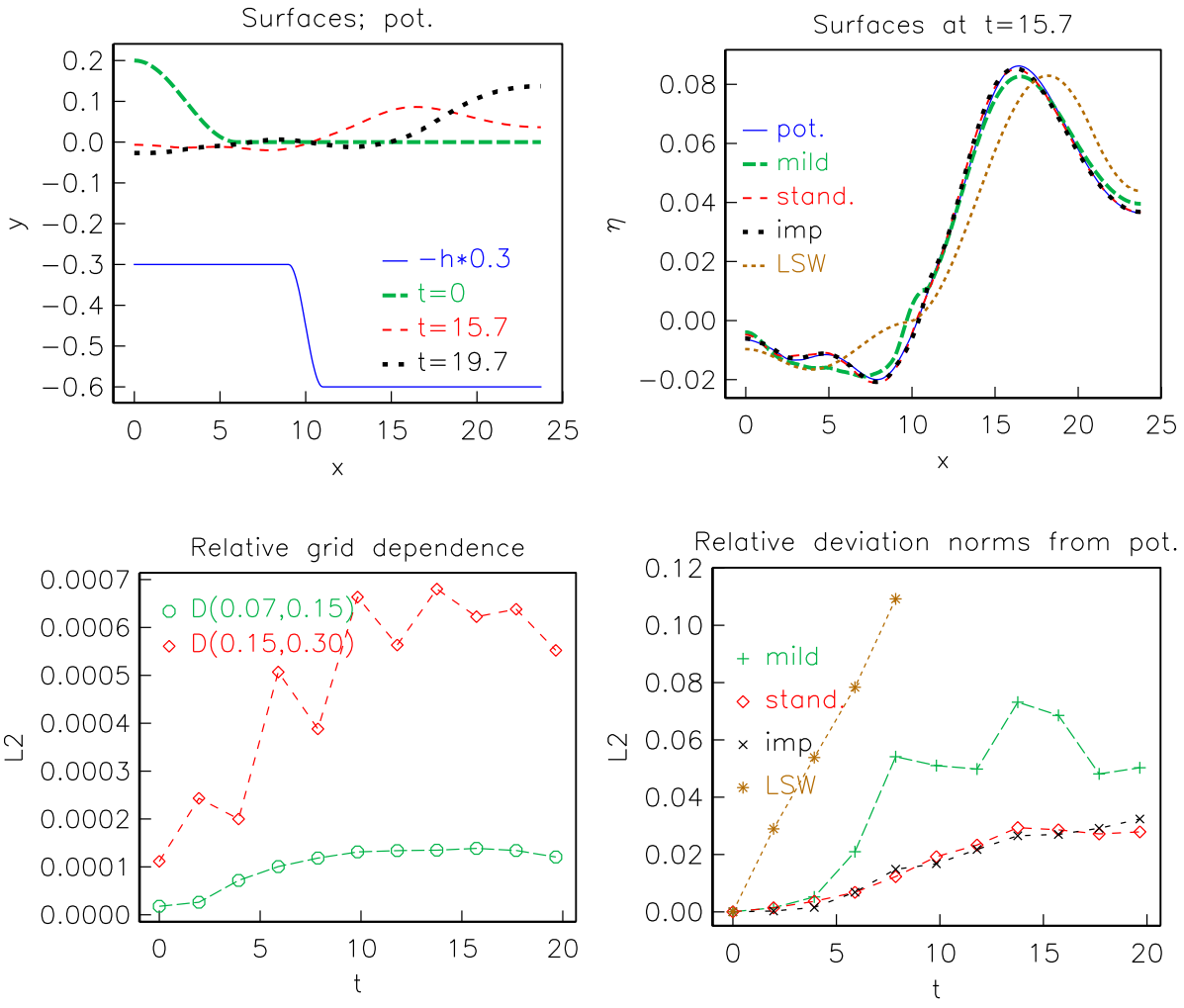

Figure 10: Comparison of linear Boussinesq and full potential models for $\boldsymbol{A} = \mathbf{0.2}$, $\boldsymbol{\lambda} = \mathbf{12.0}$, $\boldsymbol{\ell} = \mathbf{2}$, $\boldsymbol{h_r} = \mathbf{2}$, $\boldsymbol{x_r} = \mathbf{9.0}$, $\boldsymbol{x_{\max}} = \mathbf{23.7}$, $\boldsymbol{\Delta x} = \mathbf{0.07}$ (mild). Upper left panel: surfaces at given times and the bottom. Upper right panel: comparison of different solvers at $t = 15.7$. Lower left panel: convergence of potential model; evolution of relative errors. Lower right panel: difference between other models and the potential theory.

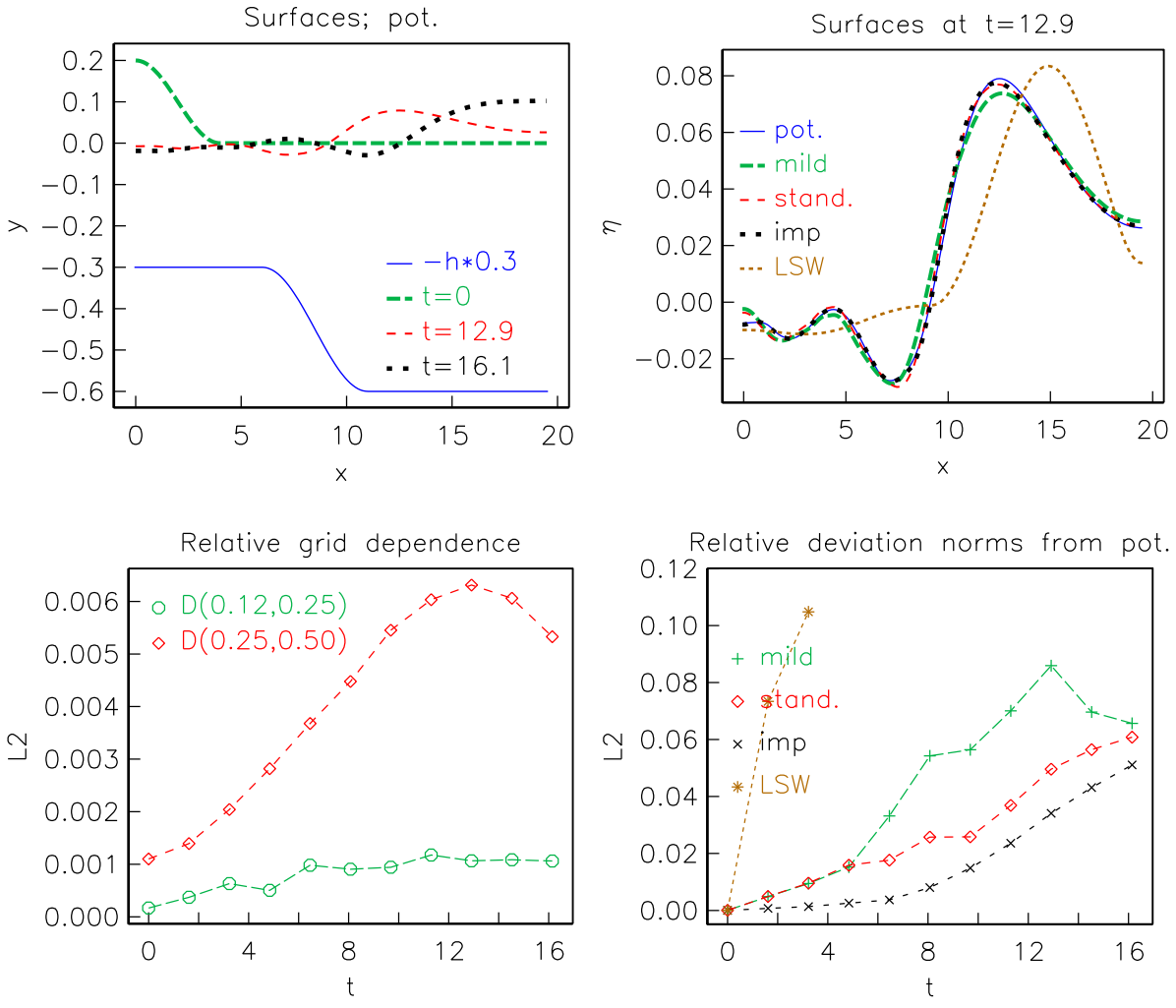

Figure 11: Comparison of linear Boussinesq and full potential models for $\boldsymbol{A = 0.2,\ \lambda = 8.0,\ \ell = 5,\ h_r = 2,\ x_r = 6.0,\ x_{max} = 19.5,\ \Delta x = 0.12}$ (mild). Upper left panel: surfaces at given times and the bottom. Upper right panel: comparison of different solvers at $t = 12.9$. Lower left panel: convergence of potential model; evolution of relative errors. Lower right panel: difference between other models and the potential theory.

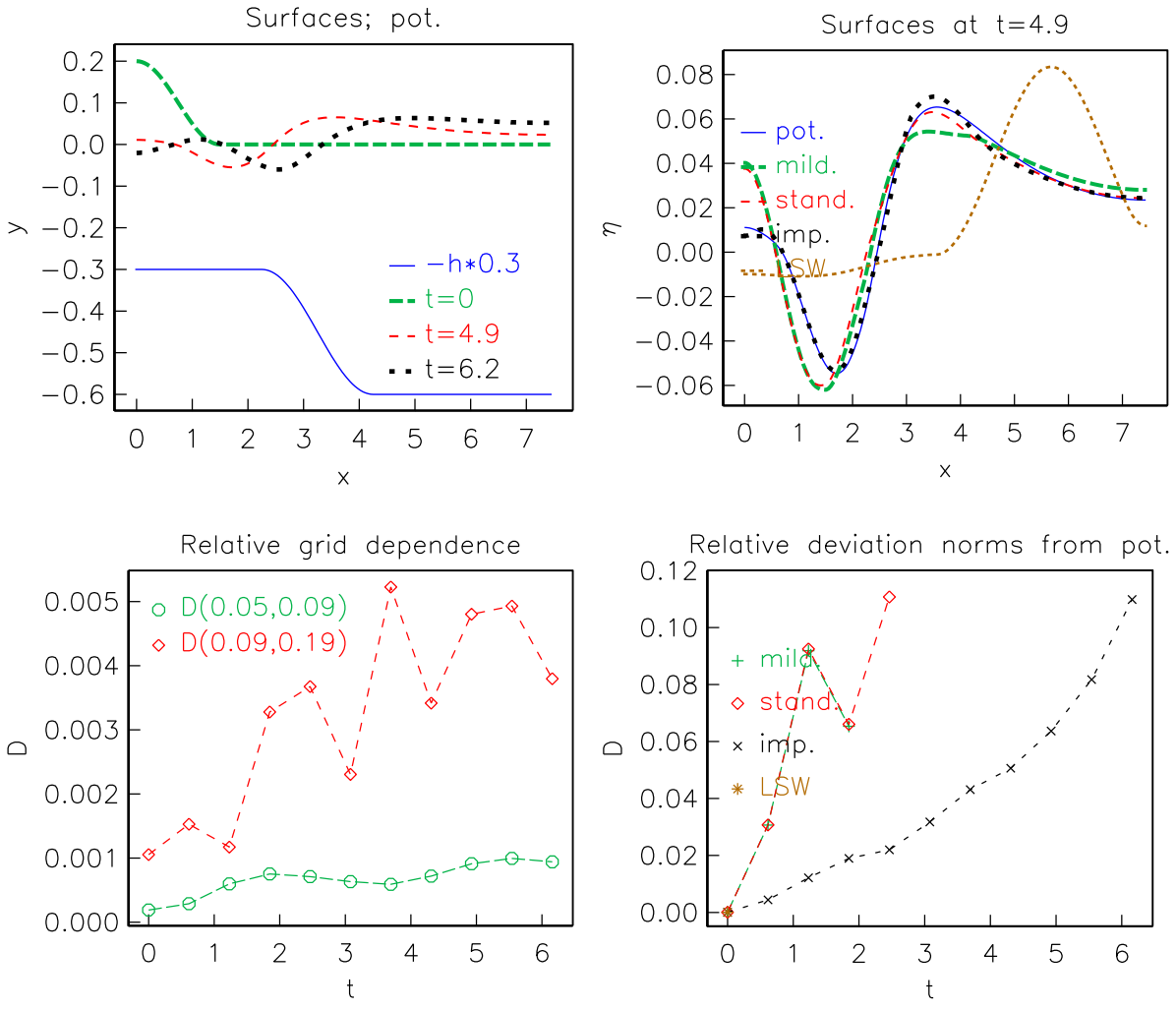

Figure 12: Comparison of linear Boussinesq and full potential models for $\boldsymbol{A} = \mathbf{0.2}$, $\boldsymbol{\lambda} = \mathbf{3.0}$, $\boldsymbol{\ell} = \mathbf{2}$, $\boldsymbol{h_r} = \mathbf{2}$, $\boldsymbol{x_r} = \mathbf{2.3}$, $\boldsymbol{x_{\max}} = \mathbf{7.4}$, $\boldsymbol{\Delta x} = \mathbf{0.05}$ (mild.). Upper left panel: surfaces at given times and the bottom. Upper right panel: comparison of different solvers at $t = 4.9$. Lower left panel: convergence of potential model; evolution of relative errors. Lower right panel: difference between other models and the potential theory.

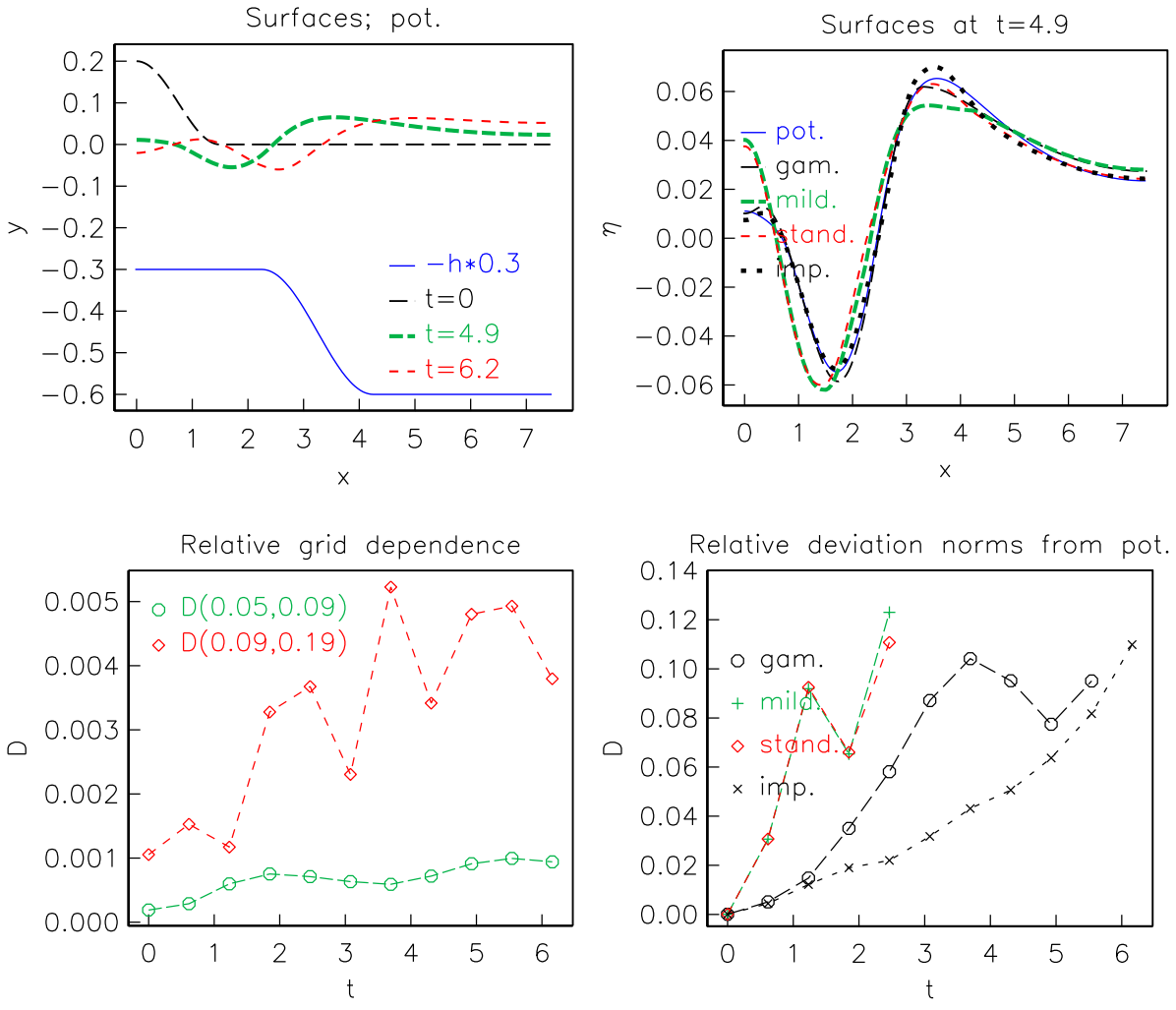

Figure 13: Comparison of linear Boussinesq and full potential models for $\boldsymbol{A = 0.2,\ \lambda = 3.0,\ \ell = 2,\ h_r = 2,\ x_r = 2.3,\ x_{\max} = 7.4,\ \Delta x = 0.05}$ (gam.). Upper left panel: surfaces at given times and the bottom. Upper right panel: comparison of different solvers at $t = 4.9$. Lower left panel: convergence of potential model; evolution of relative errors. Lower right panel: difference between other models and the potential theory.

A A boundary integral method

In the fluid the motion is goverened by the Laplace equation

$$\nabla^2\phi = 0 \quad \text{for} \quad -h < z < \eta.$$

At the free surface ($z = \eta$) the Bernoulli equation is expressed as

$$\frac{\mathrm{D}\phi}{\mathrm{D}t} - \frac{1}{2}(\nabla\phi)^2 + \eta = 0 \tag{26}$$

The kinematic condition at the surfce is written in the Lagrangian form

$$\frac{\mathrm{D}\eta}{\mathrm{D}t} = \frac{\partial\phi}{\partial z} \quad \frac{\mathrm{D}\xi}{\mathrm{D}t} = \frac{\partial\phi}{\partial x},$$

where (η, ξ) is the position of a surface particle. At rigid boundaries (bottom or sidewalls) we have

$$\frac{\partial\phi}{\partial n} = 0,$$

where n denotes the direction normal to the boundary.

This model is related to the high order technique of [2]. However, to allow more flexible boundary conditions, as sloping beaches, the high order polynomials are replaced by cubic splines for the spatial interpolation between nodes. Accordingly the order of the temporal scheme is reduced to third order accuracy. The key features then become

- Lagrangian particles are used along the free surface. At other boundaries both fixed and moving nodes may be employed
- Cauchy's formula for complex velocity ($q = u - \mathrm{i}v$) is used to produce an implicit relation between the velocity components along the surface

$$\alpha\mathrm{i}q(z_p) = \mathrm{PV}\oint_C \frac{q(z)}{z_p - z}dz \tag{27}$$

where α is the interior angle. Following [2] the integral equation (27) is rephrased in terms of the velocity components tangential and normal to the contour, denoted by $u^{(s)}$ and $v^{(s)}$, respectively. Invoking the relation

$$u^{(s)} - \mathrm{i}v^{(s)} = \mathrm{e}^{\mathrm{i}\theta}(u - iv),$$

where θ is the angle between the tangent and the x-axis, we then obtain

$$\alpha\mathrm{i}(u_p^{(s)} - v_p^{(s)}) = \mathrm{e}^{\mathrm{i}\theta_p}\mathrm{PV}\oint_C \frac{u^{(s)} - iv^{(s)}}{z_p - z}ds. \tag{28}$$

For rigid boundaries, where the normal velocity is known, the real component of this equation is imposed, while the imaginary component is used at free surfaces, where u_s is known from the integration of the Bernoulli equation. The equation set is established by collocation in the sense that z_p runs through all nodes to produce as many equations as unknowns (see figure 14).

- Cubic splines for field variables – solution is twice continuously differentiable

- Combination of Taylor series expansion and multi-step technique used for time integration. This allows for variable time stepping. For instance, ϕ_p is advanced one time step n to $n+1$ according to

$$\phi_{(n+1)} = \phi_{(n)} + \Delta t_{(n)} \left(\frac{\mathrm{D}\phi}{\mathrm{D}t}\right)_{(n)} + \frac{1}{2}\Delta t_{(n)}^2 \left(\frac{\mathrm{D}^2\phi}{\mathrm{D}t^2}\right)_{(n)} + \frac{1}{6}\frac{\Delta t_{(n)}^3}{\Delta t_{(n-1)}} \left(\frac{\mathrm{D}^2\phi}{\mathrm{D}t^2}_{(n)} - \frac{\mathrm{D}^2\phi}{\mathrm{D}t^2}_{(n-1)}\right).$$

  The last, backward difference both increases the accuracy and stabilize the scheme. The first temporal derivative of ϕ is obtained from the Bernoulli equation. We then also obtain the local derivative, $\frac{\partial\phi}{\partial t}$, that is used to define a boundary value problem for the temporal derivatives of the velocity. This is identical to the problem for the velocities themselves, given by (27) or (28) with u and v replaced by their local time derivatives. Formulas like the one above are applied to the other principal unknowns ξ and η.

- Special treatment of corner points; invocation of analyticity.

- Like most models of this kind some filtering is required in the nonlinear case to avoid growth of noise. A five point smoothing formula is applied to this end.

In sum we have a "moderately high order" method that is lower order compared to the method [2], but at the same time less restricted at the boundaries.

The computational cycle consists of the following main steps

1. We know velocities (and more) at t. Time stepping by discrete surface condition give ϕ (potential) and particle positions at the surface for $t+\Delta t$

2. ϕ at surface yields the tangential velocity at the surface

3. Crucial step: Tangential velocity at surface and bottom condition (normal velocities) yield equations for the other velocity component through the integral equation (28) that is equivalent to the Laplace equation

4. $\partial\phi/\partial t$ is obtained from the Bernoulli equation (26). The tangential component of the temporal derivative of the velocity is then obtained, in analogy to step 2, and the linear equation set from step 3 is solved with a new right hand side to obtain the remaining component of $\partial\mathbf{v}/\partial t$.

5. The Bernoulli equation is differensiated, materially, with respect to t and $\frac{\mathrm{D}^2\phi}{\mathrm{D}t^2}$ is computed.

6. Now the first and second order Lagrangian derivatives of ϕ, ξ and η are computed at $t+\Delta t$ and the cycle may repeat itself.

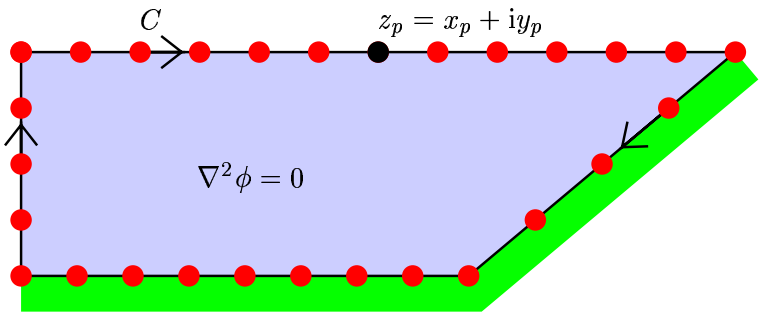

Figure 14: Definition sketch of computational domain in BEM method

The whole problem is then posed in terms of the position of the fluid boundary and the velocity potential there. Values of velocities within the fluid may be obtained by choosing z_p as an interior point and put $\alpha = 2\pi$ in the Cauchy relation (27), which then provide explicit expressions for u_p and v_p. In the linear case the procedure is substantially soimplified since the geomtry is constant and matrices involved in the third step may be computed and factorized only once.

References

[1] X. Chen and S. Sharma. A slender ship moving at a near-critical speed in a shallow channel. *J. Fluid Mech.*, 291:263–285, 1995.

[2] J. W. Dold. An efficient surface-integral algorithm applied to unsteady gravity waves. *J. Comp. Phys.*, 103:90–115, 1992.

[3] Wei G., Kirby J. T., Grilli S. T., and Subramanya R. A fully nonlinear boussinesq model for surface waves. part 1. highly nonlinear unsteady waves. *J. Fluid Mech.*, 294:71–92, 1995.

[4] S.-H. Hsiao, P. L.-F. Liu, and Y. Chen. Nonlinear water waves propagating over a permeable bed. *Phil. Trans. R. Soc. Lond. A*, 458:1291–1322, 2002.

[5] A. B. Kennedy, Q. Chen, J. T. Kirby, and R. A. Dalrymple. Boussinesq modeling of wave transformation, breaking, and run-up. Part I: 1D. *J. Waterw., Port, Coast., Ocean Engrg.*, 126(1):39–47, 2000.

[6] H. P. Langtangen and G. Pedersen. Computational models for weakly dispersive nonlinear water waves. *Comp. Meth. Appl. Mech. Engrg.*, 160:337–358, 1998.

[7] P. A. Madsen and H. A. Schäffer. A review of Boussinesq-type equations for surface gravity waves. volume 5 of *Advances in Coastal and Ocean Engineering*, pages 1–95. World Scientific Publishing Co., Singapore, 1999.

[8] C. C. Mei. *The Applied Dynamics of Ocean Surface Waves*. World Scientific, 1989.

[9] O. Nwogu. Alternative form of Boussinesq equations for nearshore wave propagation. *J. Waterw., Port, Coast., Ocean Engrg.*, 119(6):618–638, 1993.

[10] G. Pedersen. On the numerical solution of the Boussinesq equations. Preprint series in applied mathematics, Dept. of Mathematics, University of Oslo, 1988.

[11] G. Pedersen. Energy conservation and physical optics for discrete long wave equations. *Wave Motion*, 37:81–100, 2003.

[12] D. H. Peregrine. Equations for water waves and the approximation behind them. In R. E. Meyer, editor, *Waves on beaches*, pages 357–412. Academic Press, New York, 1972.

[13] T. Y. Wu. Long waves in ocean and coastal waters. *Proc. ASCE, J. Eng. Mech. Div.*, 107:501–522, 1981.